Chapter 5

Effect of Mn incorporation in $KCo_{1-x}Ni_xPO_4$ ($0 \leq x \leq 0.5$) Electrodes for development of high performing electrodes for Hybrid Supercapacitors

5.1 Introduction

The dependence on fossil fuels to produce electricity has resulted in huge environmental challenges, including greenhouse gas emissions and the eventual depletion of these finite resources. Transitioning Toward Sustainable Energy Storage Solutions makes clean and sustainable energy solutions an imperative necessity, especially considering the intermittency of renewable energy sources such as solar and wind. Electrochemical energy storage devices (EESDs) are promising technologies to overcome these challenges through the efficient storage of renewable sources of energy for continuous use.[1]-[4]

Batteries and Supercapacitors are the two primary options for energy storage. Although they have high energy density to be used for long durations in storage, batteries suffer with the inability to provide high power densities because of the slow nature of the faradaic charge storage process. Super-capacitors, meanwhile, provide high power density and fast charge-discharge cycles through electrostatic energy storage but have very much inferior energy densities, which limit their scope for long-term applications. [5]-[8]

Traditional Supercapacitors have poor energy density and long-term stability. Advances in the form of Hybrid or Asymmetric Supercapacitors have been able to overcome these drawbacks by combining faradic and capacitive processes. Aqueous Asymmetric Supercapacitors (AASCs) are of particular interest because they employ safer, more environmentally friendly aqueous electrolytes and exhibit greater specific capacitance than their conventional electric double-layer capacitors (EDLCs). AASCs also feature a characteristic diagonal Ragone plot, showing that they can simultaneously achieve high power and energy densities.[7][11][12]

Although there has been considerable advancement, these Supercapacitors face severe drawbacks in the form of poor cycle stability, low specific energy, and deterioration during rapid charge-discharge cycles. It requires novel material design incorporating a high level of conductivity, a large surface area, and superior electrochemical stability.

This technology gap has filled with Hybrid Supercapacitors (HSCs). Integrating both a battery-type electrode that provides for higher energy density and a capacitive electrode which provides the requirements for power density and cycling stability, HSCs deliver the best from both the worlds. The system which includes the renewable energy sources, electric cars, or even portable electronic devices that can apply the Hybrid Supercapacitors (HSCs). [8–10]

The electrode materials are highly essential for the performance of the Supercapacitors and Hybrid devices. Carbon-based materials are the most dominant negative electrodes due to a high-power density and long cycles. Transition metal-based compounds, including polyanion framework materials, are commonly used as positive electrodes, which offer excellent structural stability, high redox potential, and also thermal resilience.[15]

The most promising ones have a structure of covalently bonded $(XO_4)n-$ tetrahedra, where X = P, S, B, C, Si, etc., and M-O polyhedral subunits, where M = Fe, Ni, Mn, Co, Ti, V, Cr, etc. An open-pore structure can allow for easy transport of ions, while the presence of strong X-O bonds will provide thermal stability along with minimal volume expansion. For instance, phosphates based on cobalt offer good redox activity, sustainability, and environmental friendliness and can be used for energy storage. [16],[18]

The realization of the maximum potential of next-generation Supercapacitors will demand significant research efforts on new electrode materials and device architectures. Nanostructured materials, metal oxides, carbon-based composites, and Hybrid materials have good prospects for improvements in energy density, charge-discharge efficiency, and cycle life. The strategic integration of nickel and manganese with cobalt materials also has the potential to improve electrochemical performance and structure stability as the number of active redox sites is increased. [15,20]

With further development, Hybrid and Asymmetric Supercapacitors will find their way to be one of the cornerstones of the transition towards sustainable energy systems, including applications ranging from grid-scale storage to electric vehicles and portable electronics.[15][21]

The current work focuses on synthesis, characterization and electrochemical charge storage performance of the Nickel and Manganese substituted, Potassium Cobalt phosphate,[14] $KCo_{0.5}Ni_{0.4}Mn_{0.1}PO_4$, with a possible promising positive electrode material, specifically for the Asymmetric Supercapacitor (ASCs) in Full Cell configuration. Electrochemical performance of $KCo_{0.5}Ni_{0.4}Mn_{0.1}PO_4$ increased substantially due to the interaction of Cobalt, Nickel, and Manganese in synergistic manner. Specifically, it offered a charge capacity of 231.7 mAh/g that is equivalent to 521.32 F/g capacitance, at 1 A/g current density within voltage of 0-1.6V by using a 2M KOH aqueous electrolyte. The product maintained cyclic stability up to 5000 cycles.

In Hybrid Supercapacitor (HSC) mode, where Activated Carbon is used as the negative electrode and $KCo_{0.5}Ni_{0.4}Mn_{0.1}PO_4$ as the positive electrode, the system obtained an impressive energy density of 202.7 Wh/kg and power density of 9642 W/kg in 2M aqueous KOH electrolyte. These results indicate the potential of $KCo_{0.5}Ni_{0.4}Mn_{0.1}PO_4$ as a robust and high-performance positive electrode material for advanced HSCs development.

5.2 Material Synthesis and characterization

5.2.1 Synthesis of $KCo_{0.5}Ni_{0.4}Mn_{0.1}PO_4$

The $KCo_{0.5}Ni_{0.4}Mn_{0.1}PO_4$ was synthesized using a sol-gel auto-combustion method followed by high-temperature calcination. All chemicals used were of analytical grade and used without purification. Precursors used were Nickel Nitrate Hexahydrate, Merck, 99.0%, Cobalt Nitrate Hexahydrate, Merck, 99.0%, Manganese (II) acetate, Merck, 98.0%, Potassium Carbonate, Merck, 99.9%, Ammonium Phosphate, Merck, 99.0%, and Malic Acid, Merck, 99.9% which are mixed in stoichiometric molar ratios to prepare $KCo_{0.5}Ni_{0.4}Mn_{0.1}PO_4$. The quantity of malic acid employed was twice the moles combined of the Co, Ni, Mn, and K precursors.

To prepare $KCo_{0.5}Ni_{0.4}Mn_{0.1}PO_4$ by adding Solution A to a reaction solution containing Solution B. Prepare Solution A by adding 0.5mM Nickel Nitrate Hexahydrate, 0.5mM Cobalt Nitrate Hexahydrate, 0.1mM Manganese (II) acetate and 1mM of Potassium Carbonate into 100 ml deionized water. Make a separate container for preparing Solution B, containing 1mM Ammonium Phosphate. Gradually add Solution B to Solution A then slowly add 4mM of maleic Acid. This leads to the formation of a homogenous metal-citrate complex at 100°C. The mixture is stirred continuously at 80°C for 4 hours, providing a light pinkish gel.

The temperature was raised to 200°C, and the combustion was held for about 3–5 minutes at this temperature. It created a voluminous, fluffy dark brown-colored powder. The product is ground and pre-treated inside a muffle furnace for 6 hours at a temperature of 400°C. It was then calcined in a furnace for 8 hours at a temperature of 600°C to form crystalline $KCo_{0.5}Ni_{0.4}Mn_{0.1}PO_4$. Blue color powder was collected, finely grounded, and prepared for analysis and characterization of electrochemical performances.

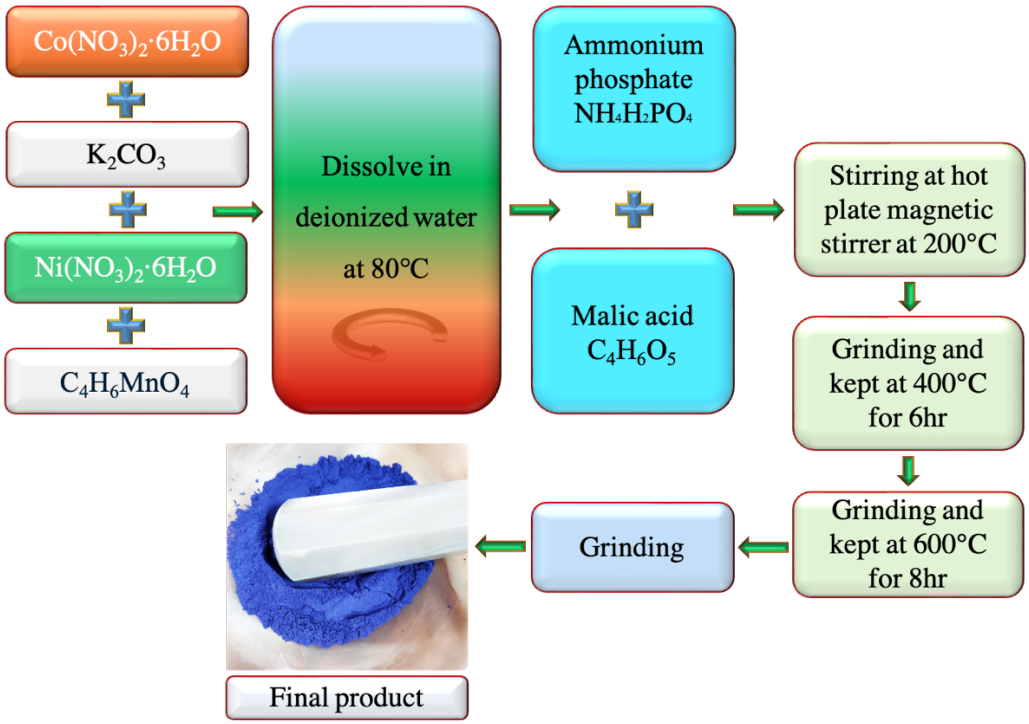

Figure 5.1: Synthesis procedure of $KCo_{0.5}Ni_{0.4}Mn_{0.1}PO_4$ sample

5.2.2 Materials characterization

The crystallinity and phase purity of $KCo_{0.5}Ni_{0.4}Mn_{0.1}PO_4$ sample were determined through powder X-ray diffraction (XRD). The measurements were carried out with monochromatic Cu Kα radiation (λ = 1.54056 Å) on a Rigaku Miniflex 600 benchtop X-ray diffractometer in the range of 2θ between 10–60° and a step size of 0.02°. Structural identification was performed using X'Pert HighScore Plus (PANalytical) software, and further crystal structure refinement was carried out using Rietveld refinement with FullProf Suite software.

The morphology of the synthesized $KCo_{0.5}Ni_{0.4}Mn_{0.1}PO_4$ sample was characterized by using an EVO Scanning Electron Microscope (MA15/18, CARL ZEISS).

X-ray photoelectron spectroscopy (XPS) was used to determine the elemental composition and electronic states of the sample, using a Thermo Scientific instrument with a monochromatic Al Kα X-ray source.

5.2.3 Electrochemical Studies

To evaluate the electrochemical properties of the prepared $KCo_{0.5}Ni_{0.4}Mn_{0.1}PO_4$ sample, cyclic voltammetry (CV), galvanostatic charge-discharge (GCD), and electrochemical impedance spectroscopy (EIS) tests were carried out on a three-electrode setup. The obtained measurements were done on a Metrohm Autolab (PGSTAT204) with a FRA32M module. The NOVA1.1 software was applied for further processing of electrochemical data.

5.2.4 Electrode preparation

The experiments were conducted on a three-electrode arrangement, where $KCo_{0.5}Ni_{0.4}Mn_{0.1}PO_4$ was taken as the working electrode, while saturated calomel electrode (SCE) as the reference electrode, and the counter electrode is a platinum plate. Electrodes were prepared by mixing $KCo_{0.5}Ni_{0.4}Mn_{0.1}PO_4$, conductive carbon (acetylene black, Alfa Aesar), and binder (PVDF, Merck) at 70:20:10 weight % ratio, in a NMP (N-Methyl-2-pyrrolidone) solvent, well blended in an agate mortar and pestle until forming uniform slurry. About 1 mg of the active material was subsequently cast onto a 1 cm^2 area of Toray carbon paper (Alfa Aesar) and dried at 80 °C for 12 hours for the working electrode.

The mass of the loaded electrode was measured by taking the difference between the loaded and blank electrodes using a Shimadzu electronic balance with a resolution of 0.01 mg. The dry electrodes were then subjected to electrochemical characterization. For full-cell measurements, Activated Carbon was used both as counter and reference electrode in a 2M KOH electrolyte for Hybrid Supercapacitors.

5.3 Result and discussion

5.3.1 X-ray diffraction (XRD) analysis

XRD patterns of powder sample $KCo_{0.5}Ni_{0.4}Mn_{0.1}PO_4$ calcined at 600°C, agree well with those of JCPDS No. 82-0762 associated with hexagonal $KCoPO_4$. The Rietveld-refined powder XRD profile for calcined $KCo_{0.5}Ni_{0.4}Mn_{0.1}PO_4$, as shown in **figure 5.2(a)**, confirms a good match with the reference structure (JCPDS No. 82-0762) without the presence of any detectable impurity peaks. The lattice parameters, after refinement, are a = 18.01 Å, b = 18.01 Å, c = 8.60 Å, and reliability factors are Rp = 15.12, R_{wp} = 10.58, and R_{exp} = 8.15 with χ^2 = 1.93; the formation of hexagonal crystal structure belonging to space group $P6_3$ is established.

The presence of Co-O, Ni-O, and Mn-O polyhedral units, which are connected to each other through corner-sharing phosphate oxygen atoms, is validated from the VESTA image in **figure 5.2(b)**. The replacement of Co^{2+} ions having an ionic radius of 0.58 Å at tetrahedral sites by Ni^{2+} ions having an ionic radius of 0.55 Å Mn^{2+} ions having an ionic radius of 0.66 Å shifts the peak toward a higher angle. The calculated crystallite size reduced due to this peak shift, as determined using Debye-Scherrer's equation.[14][22]

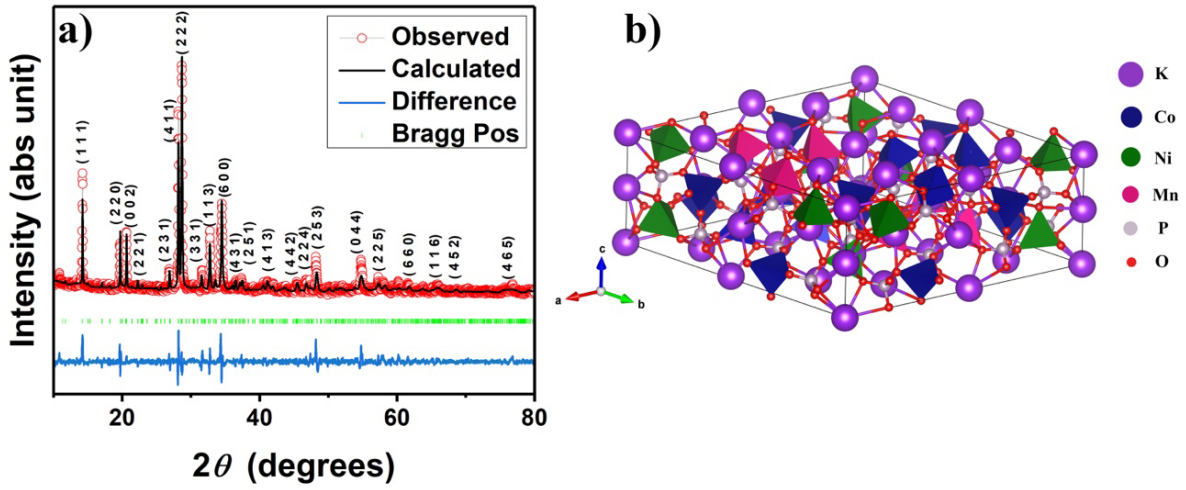

Figure 5.2: (a) XRD Rietveld refinement pattern of $KCo_{0.5}Ni_{0.4}Mn_{0.1}PO_4$ powder sample (b) VESTA image of $KCo_{0.5}Ni_{0.4}Mn_{0.1}PO_4$ (blue, green, pink,grey are tetrahedra of Co-O, Ni-O, Mn-O and P-O, respectively)

5.3.2 X-ray photoelectron spectroscopy (XPS) Analysis

Chemical composition and valence states of elements present in the sample $KCo_{0.5}Ni_{0.4}Mn_{0.1}PO_4$ are analyzed through XPS (X-ray photoelectron spectroscopy) shown in **figure (5.3)**. Broad survey spectrum in **figure 5.3(a)** supports the existence of K, Co, Ni, Mn, P, and O in the sample. From **figure 5.3(b)**, the two binding energies of K $2p_{3/2}$ and K $2p_{1/2}$ were observed at the binding energy value of 292.2 eV and 295.1 eV, which confirm the presence of K^+ ions in the compound.

The Co(2p) spectrum in **figure 5.3(c)** splits into peaks with separations associated with the $2p_{3/2}$ state of Co^{2+} at 780.63 eV and the $2p2p_{1/2}$ state at 796.41 eV. In addition to the peaks associated with Co^{2+} ions, satellite peaks appear at 784.17 eV and 801.96 eV. In the Ni(2p) core level spectrum, shown in **figure 5.3(d)**, the Ni $2p_{3/2}$ and Ni $2p_{1/2}$ states are found to correspond to binding energies of 855.6 eV and 873.4 eV, respectively. Each state is accompanied by satellite peaks at 860.9 eV and 879 eV. All the aforesaid values ascertain that the sample contains Ni as Ni^{2+}.

Figure 5.3(e) displays the Mn(2p) spectrum state of the $KCo_{0.5}Ni_{0.4}Mn_{0.1}PO_4$ with two evident peaks of Mn $2p_{1/2}$ and Mn $2p_{3/2}$ states are found to correspond to binding energies of 639.6 eV and 651.4 eV, respectively. Mn $2p_{3/2}$ state is accompanied by satellite peak at 644.6 eV, all the aforesaid values confirm the presence of Mn^{2+} ions in the compound.

Figure 5.3(f) displays the O(1s) spectrum state of the $KCo_{0.5}Ni_{0.5}PO_4$ with two evident peaks at 530.8 eV corresponding to metal-oxygen bonds Ni-O and Co-O while the second peak is situated at 532.2 eV related to P-O bonds.[23] Finally, **Figure 5.3(g)** P(2p) is split into the P $2p_{3/2}$ and P $2p_{1/2}$ states with their binding energies at 132.41 eV and 133.47 eV, which confirms the presence of P^{5+} ions within the PO_4 unit.

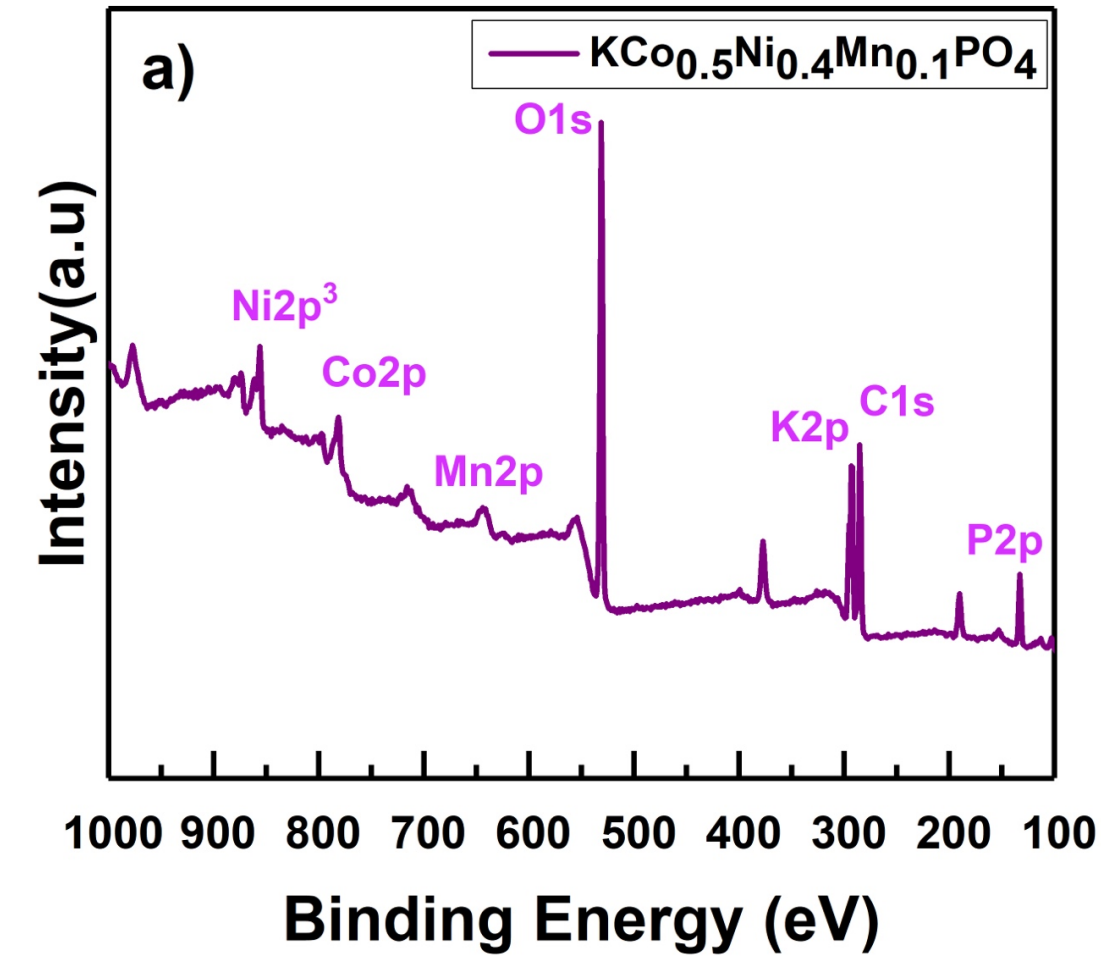
a)
KCo0.5Ni0.4Mn0.1PO4
O1s
Ni2p3
Co2p
Mn2p
K2p
C1s
P2p
Intensity(a.u)
1000 900 800 700 600 500 400 300 200 100
Binding Energy (eV)

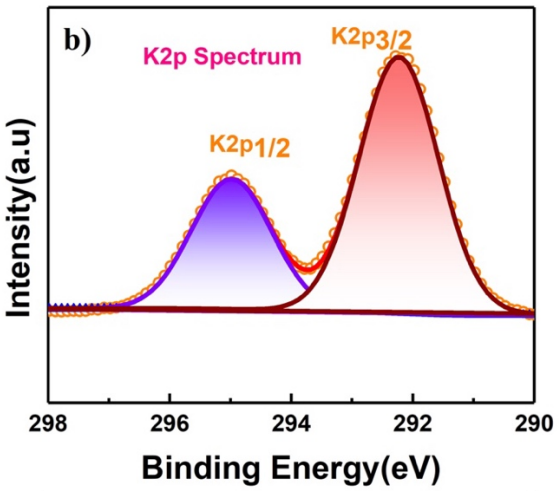
b)
K2p Spectrum
K2p3/2
K2p1/2
Intensity(a.u)
298 296 294 292 290
Binding Energy(eV)

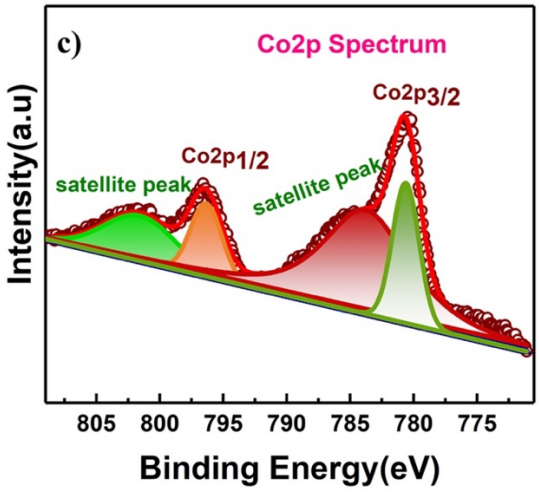
c)
Co2p Spectrum
Co2p3/2
Co2p1/2
satellite peak
satellite peak
Intensity(a.u)
805 800 795 790 785 780 775
Binding Energy(eV)

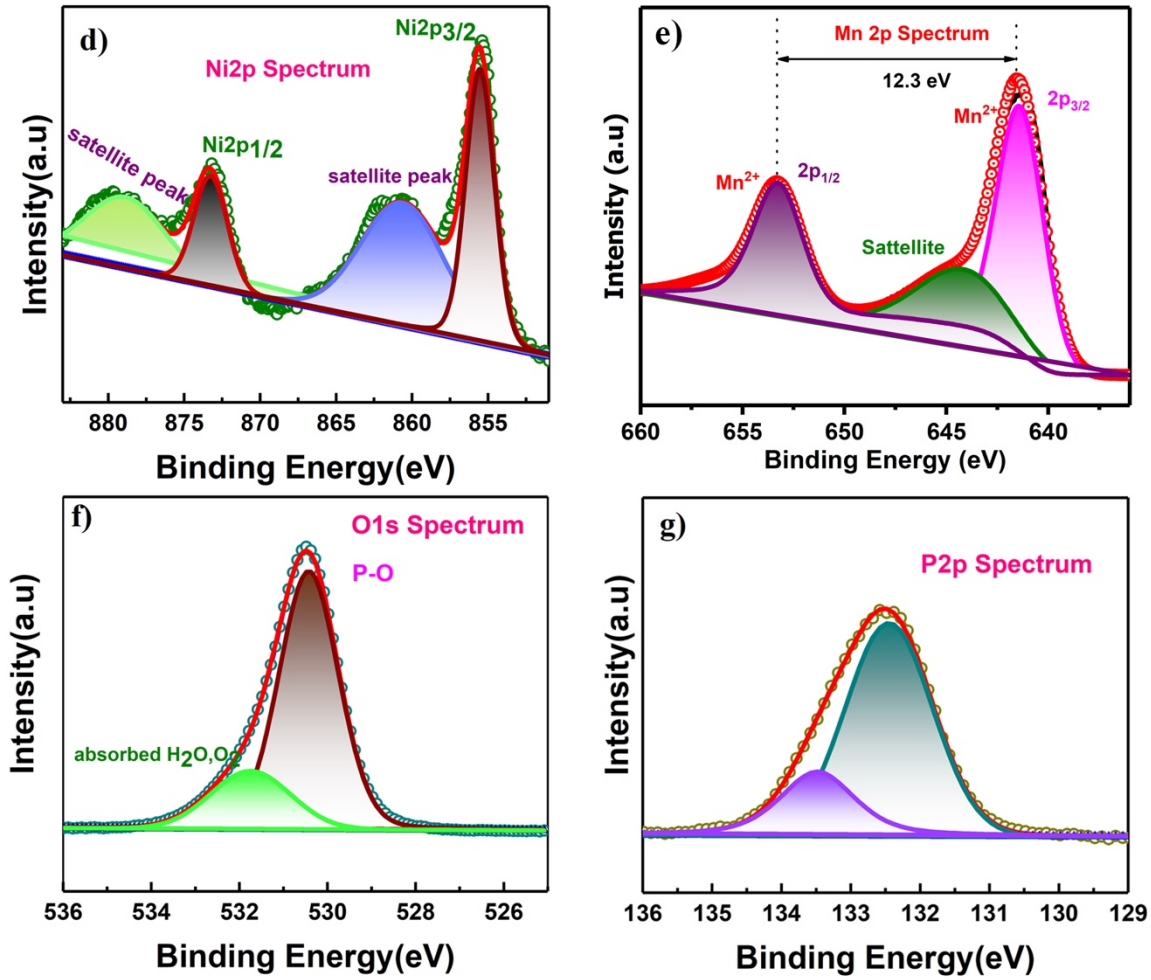

Figure 5.3: XPS of $KCo_{0.5}Ni_{0.4}Mn_{0.1}PO_4$ of powder sample; (a) full survey, (b) K (1s), (c) Co(2p), (d) Ni(2p), (e) Mn (2p) and (f) O (1s) (g) P(2p)

5.3.3 SEM and EDAX Analysis

The synthesized $KCo_{0.5}Ni_{0.4}Mn_{0.1}PO_4$ sample were characterized for their morphological properties using electron microscopy techniques. **Figure 5.4(a)** is the FE-SEM image of the $KCo_{0.5}Ni_{0.4}Mn_{0.1}PO_4$ sample that depicts a polyhedral morphology particle morphology. **Figure 5.4(b)** is the Energy Dispersive X-ray Analysis of the elemental composition of $KCo_{0.5}Ni_{0.4}Mn_{0.1}PO_4$ that indicates the presence of K, Co, Ni, Mn, P, and O elements. Besides, FE-SEM mapping images in **figures 5.4(c-h)** confirm the even distribution of these elements

across the electrode material, indicating they are present in their pure forms in the synthesized product.

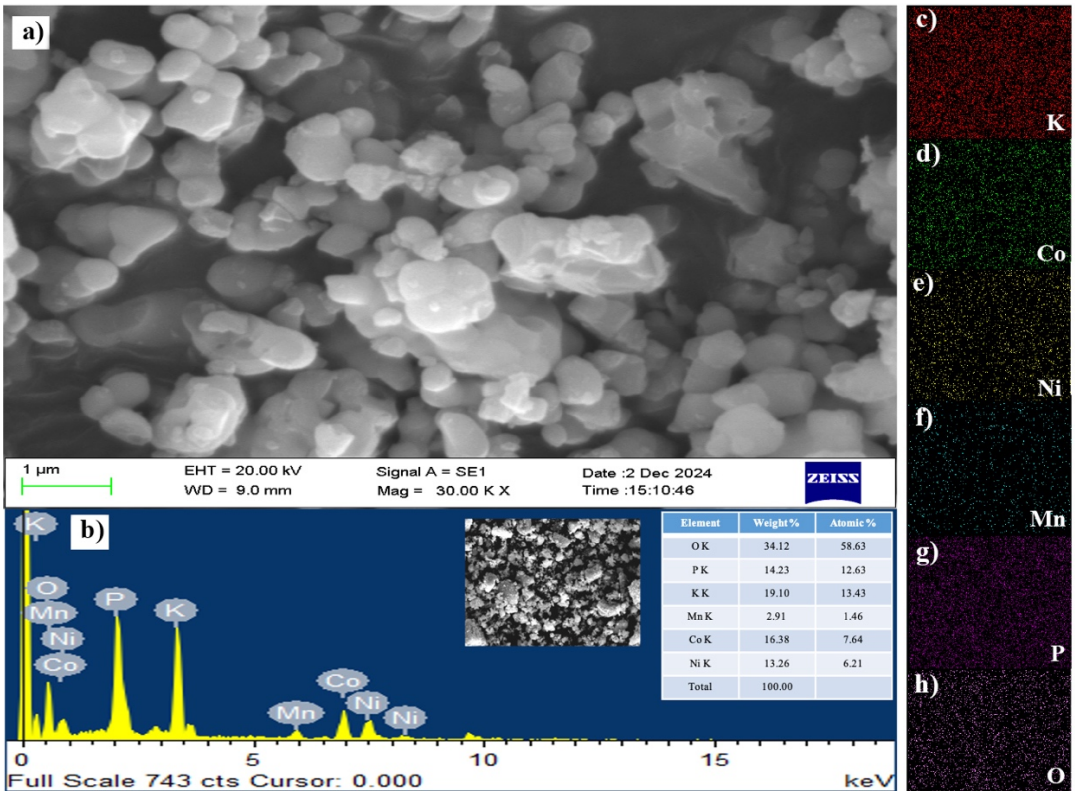

Figure 5.4: (a) SEM image of $KCo_{0.5}Ni_{0.4}Mn_{0.1}PO_4$ sample, (b) elemental analysis of $KCo_{0.5}Ni_{0.4}Mn_{0.1}PO_4$ by EDX. (c)-(h) Colour mapping of the element present in $KCo_{0.5}Ni_{0.4}Mn_{0.1}PO_4$

5.4 Electrochemical Studies:

5.4.1. Half-cell (three-electrode electrochemical cell) measurements

Figure 5.5, presented the CV curves of the $KCoPO_4$, $KCo_{0.5}Ni_{0.5}PO_4$, and $KCo_{0.5}Ni_{0.4}Mn_{0.1}PO_4$ samples in 2 M KOH solution at a 5 mV/s sweep rate in a sweeping potential window of 0-0.6 V. The CV curve for $KCoPO_4$, the shape is nearly rectangular indicating capacitive type of charge storage. At all doped levels redox peaks emerged with increase in the intensity. With

increased Ni content, these peaks are more intensified with a larger area under the CV curve, which indicates enhanced charge storage capacity in the Ni-doped $KCoPO_4$ samples. With the addition of Mn content, the redox peaks (anodic and cathodic) come closer as compare to $KCo_{0.5}Ni_{0.5}PO_4$ towards the high potential which indicates that Mn doping provides structural stability.

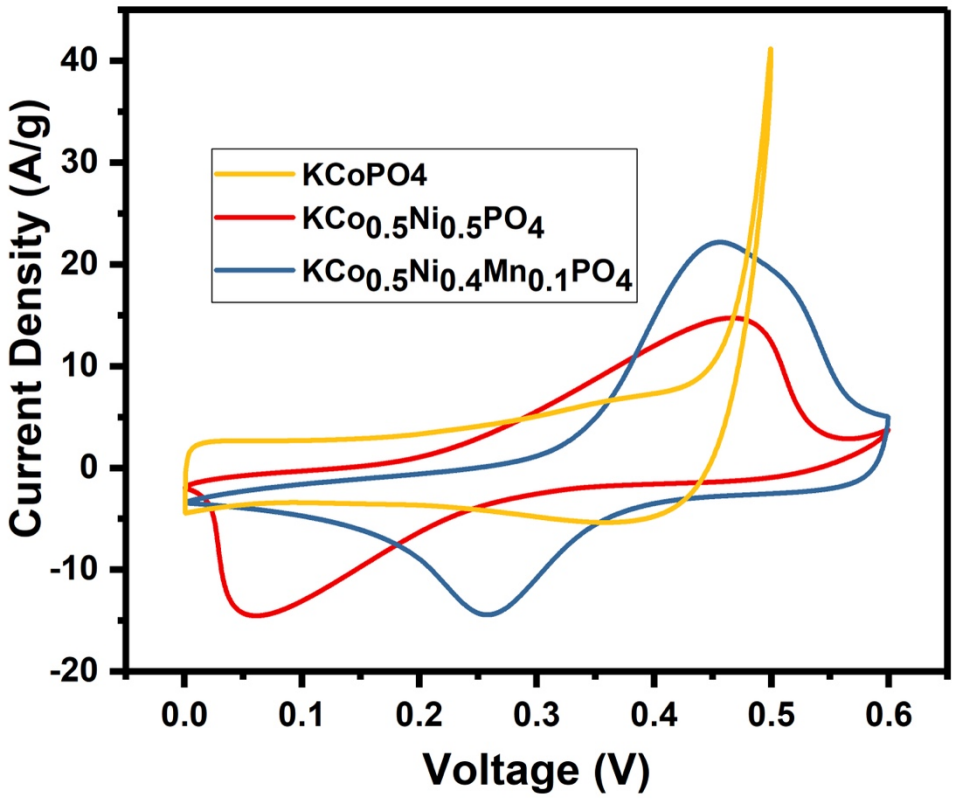

Figure 5.5: comparison CV plots of all the $KCoPO_4$, $KCo_{0.5}Ni_{0.5}PO_4$ and $KCo_{0.5}Ni_{0.4}Mn_{0.1}PO_4$ sample in 2M KOH Electrolyte for comparison at the scan rate of 5mV/s

The electrochemical properties of the samples were evaluated using charge storage capacity by Equation (5.1).

$$\text{Csp} = \frac{\int \text{i (V)dV}}{2\text{mV}\vartheta} \qquad (5.1)$$

The specific charge storage capacity in mAh/g can be calculated using eq. (5.2).

$$C\left(\frac{mAh}{g}\right) = Csp * \Delta V = \frac{\int i\,(V)dV}{2m\vartheta * 3.6} \qquad (5.2)$$

Where 'm' is the active mass of the electrode (g), 'V' is the operating voltage window (V), and 'ϑ' is the scan rate (mV/s).

The CV curves of $KCo_{0.5}Ni_{0.4}Mn_{0.1}PO_4$ at different scan rates of 1mV/s to 5mV/s are shown in **figure 5.6**. It is noted that there are two evident redox peaks within the potential range of 0 V to 0.6 V. This means that the curves are showing the combination of redox-mediated intercalation storage and surface redox (electrosorption) behavior. This confirms that charge storage occurs via an intercalative redox-mediated mechanism. The observed redox peaks are due to the reversible transitions of Co Co^{2+}/Co^{3+}, Ni^{2+}/Ni^{3+} and Mn^{2+}/Mn^{3+} as facilitated by the electrosorption of OH^- ions as described in equation (5.3).

redox-mediated diffusion-controlled intercalation reaction

$$KCo_{0.5}(II)Ni_{0.4}(II)\,Mn((II))_{0.1}\,PO_4 + OH^-_{sol} \leftrightarrow KCo_{0.5}(III)Ni_{0.5}(III)\,Mn(III)_{0.1}\,(OH^-)PO_4 + e^- \quad (5.3)$$

EDLC-type surface capacitance reaction

$$KCo_{0.5}(II)Ni_{0.4}(II)\,Mn(II)_{0.1}\,PO_4 + xKOH \leftrightarrow K^+_x \,\big|\, KCo_{0.5}(II)\,Ni_{0.4}(II)\,Mn(II)_{0.1}\,PO_4 \,\big|\, xOH^- \quad (5.4)$$

Total charge storage capacity reaction

$$KCo_{0.5}(II)Ni_{0.4}(II)\,Mn(II)_{0.1}\,PO_4 + OH^- \leftrightarrow K^+_x \,\big|\, KCo_{0.5}(II)Ni_{0.4}(II)Mn(II)_{0.1}\,PO_4 \,\big|\, OH^-_{(1+x)} + e^- \quad (5.5)$$

From the equations, (5.1) and (5.2), the charge storage capacity of $KCo_{0.5}Ni_{0.4}Mn_{0.1}PO_4$ was estimated to be approximately 158.3 mAh/g, corresponding to a capacitance of 874 F/g at a scan rate of 1 mV/s. As scan rate increased, anodic peaks as well as cathodic peaks increased; thus, it can be stated that intercalative redox process is diffusion controlled.

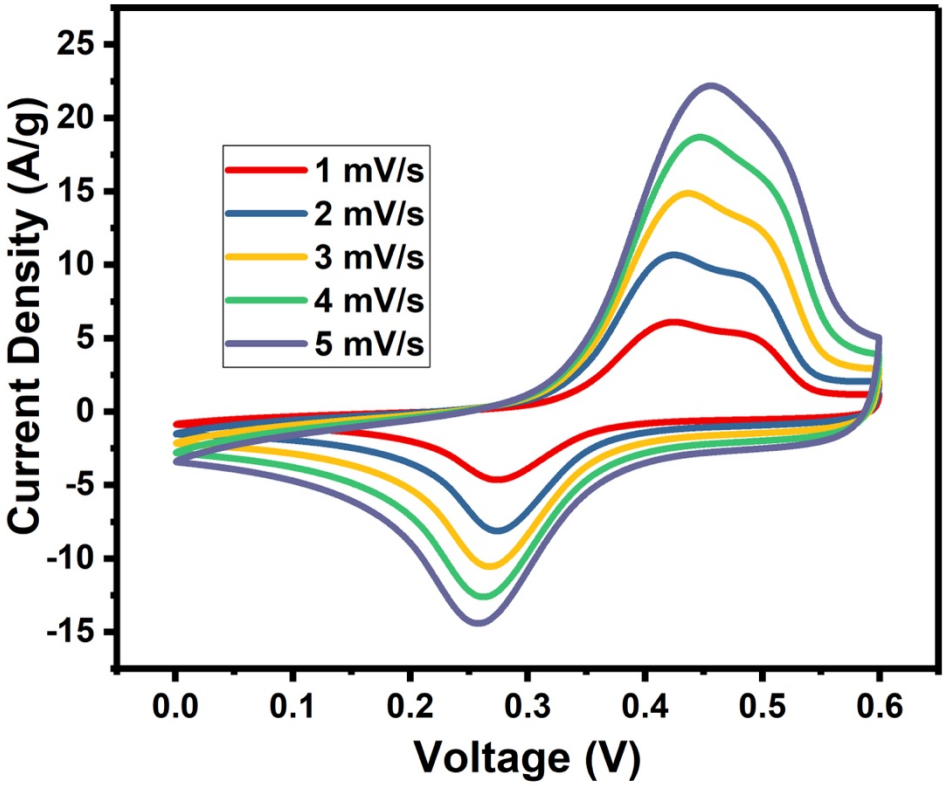

Figure 5.6: Cyclic voltammetry of $KCo_{0.5}Ni_{0.4}Mn_{0.1}PO_4$ electrode at different scan rates

GCD analysis was carried out within a voltage range of 0–0.6 V at both constant and varying current densities to further evaluate the charge storage performance. The charge storage capacity (total capacitance) of the electrode can be determined by analyzing the GCD curves at different discharge currents, using equation (5.6). [24]

$$\mathrm{Csp} = \frac{\mathrm{I}\Delta\mathrm{t}}{\mathrm{m}\Delta\mathrm{V}} \qquad (5.6)$$

The specific capacity of the electrode in mAh/g is calculated by modifying equation (4.11) as represented below.

$$C\left(\frac{mAh}{g}\right) = Csp * \Delta V = \frac{I\Delta t}{m*3.6} \qquad (5.7)$$

Where “I” is the discharge current density (A), "Δt" is the discharge time (s), m is the active mass of the electrode (g) and "ΔV" is the potential window of the discharge (V).

The galvanostatic charge/discharge (GCD) capacities of $KCo_{0.5}Ni_{0.4}Mn_{0.1}PO_4$, as shown in **figure 5.7**, were measured to be 177 mAh/g (1062 F/g), 145.6 mAh/g (873.6 F/g), 118.3 mAh/g (709.8 F/g), 106.9 mAh/g (641.4 F/g), and 58.3 mAh/g (349.8 F/g) capacities at current rates of 1, 2, 3, 4, and 5 A/g, respectively, at a voltage range of 0.6 V. The GCD curves show stable and symmetric charge/discharge characteristics, which points to the pseudocapacitive behavior of the material, driven by redox-mediated intercalation storage. In addition, the GCD results show higher capacities than cyclic voltammetry, pointing to a predominance of diffusion-controlled bulk charge storage and confirming a redox-mediated, battery-like intercalation charge storage mechanism in the material.

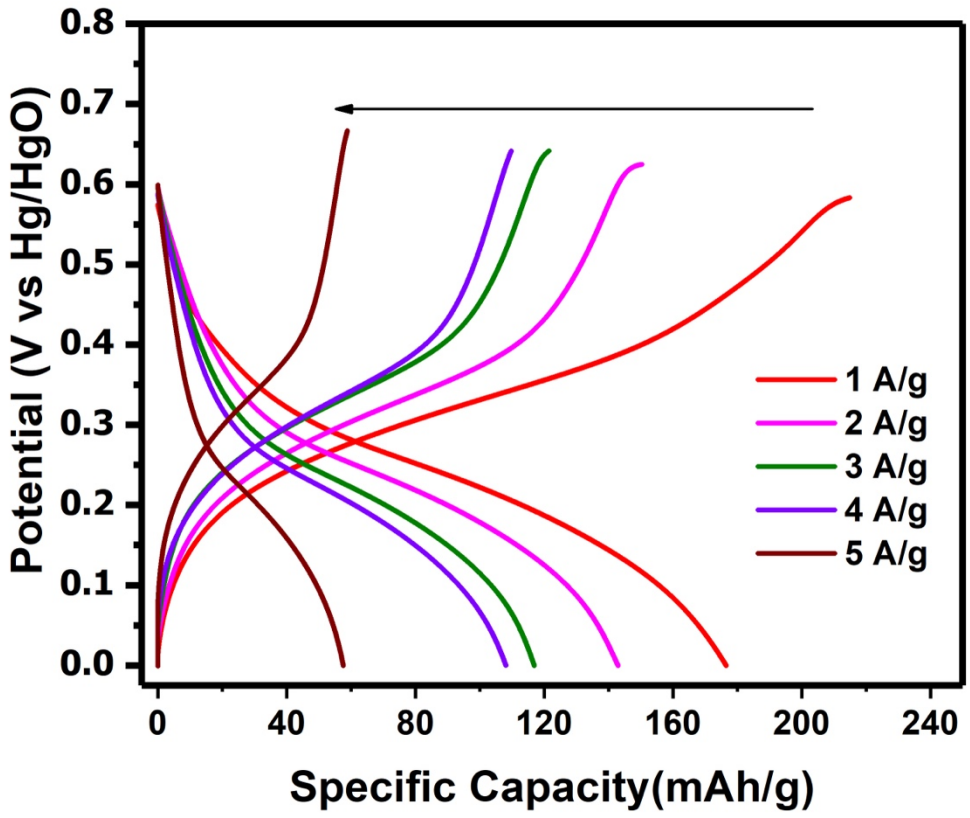

Figure 5.7: Charge/discharge specific capacity vs potential plot of the $KCo_{0.5}Ni_{0.4}Mn_{0.1}PO_4$ electrode at various constant current rates (1, 2, 3, 4 and 5A/g)

This **figure 5.8** shows a comparative charge discharge plot of all the $KCoPO_4$, $KCo_{0.5}Ni_{0.5}PO_4$ and $KCo_{0.5}Ni0.4Mn_{0.1}PO_4$ sample in 2M KOH, in which the plot of $KCoPO_4$ shows that the GCD curve is in nearly straight line which indicate the nature of $KCoPO_4$ is capacitive type and the plot of $KCo_{0.5}Ni_{0.5}PO_4$ shows a broad redox plateau of redox-mediated diffusion-controlled type, and the GCD plot of $KCo_{0.5}Ni0.4Mn_{0.1}PO_4$ shows strongly battery type nature as compare to $KCo_{0.5}Ni_{0.5}PO_4$ and also the gap between the anodic and cathodic plateau reduced which indicates that this compound is more reversible.

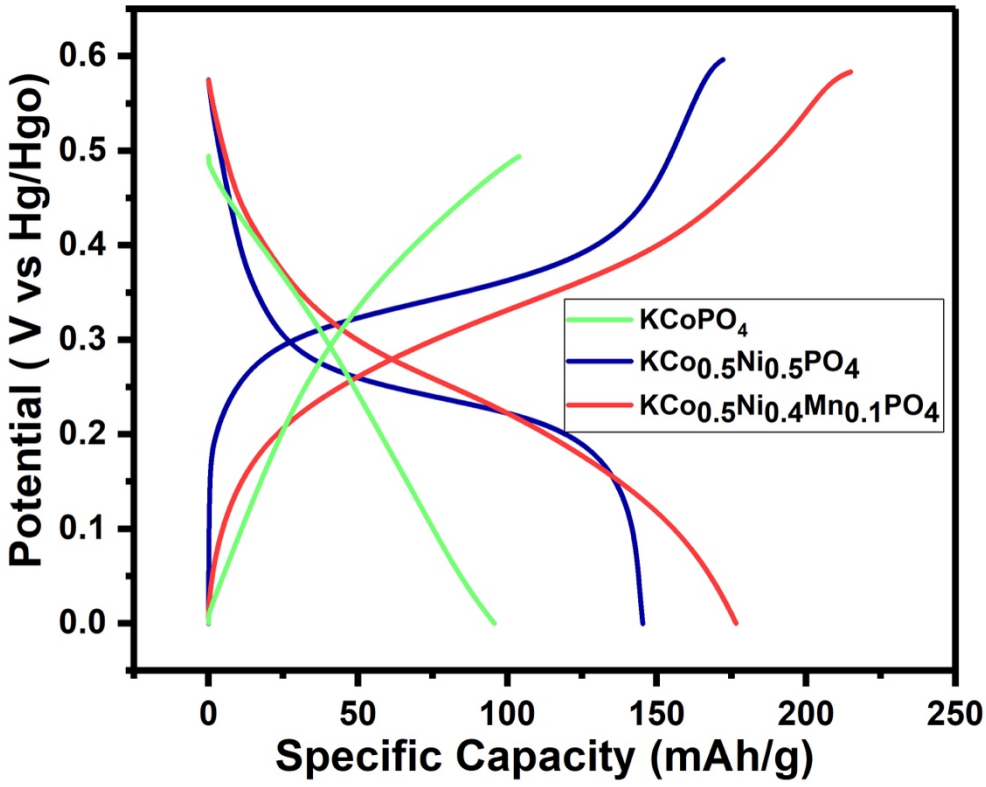

Figure 5.8: Comparative specific capacity plot of the all $KCoPO_4$, $KCo_{0.5}Ni_{0.5}PO_4$ and $KCo_{0.5}Ni_{0.4}Mn_{0.1}PO_4$ electrode at constant current rates of 1A/g

5.4.2 Full cell measurements in Hybrid Supercapacitor (HSCs) Mode

A Hybrid Supercapacitor (HSC) was fabricated using $KCo_{0.5}Ni0.4Mn_{0.1}PO_4$ as the positive electrode and Activated Carbon (AC) as the negative electrode, with a 2M KOH electrolyte to demonstrate its versatility. The charge storage capacity of both electrodes in the full-cell test will be optimized by the following equation:

$$\frac{1}{C_{total}} = \frac{1}{C_{positive}} + \frac{1}{C_{negative}} \quad (5.8)$$

In order to maintain the charge storage capacitance of each electrode in balance within the cell, the mass ratio (m+/m-) of the two electrodes was determined using the following equation (5.9):

$$\frac{m^-}{m^+} = \frac{C_+ \times \Delta E_+}{C_- \times \Delta E_-} \quad (5.9)$$

Where $m^+, m^-, C_+, C_-, \Delta E_+, \Delta E_-$ are both electrodes' active mass, specific capacitance, and potential window.

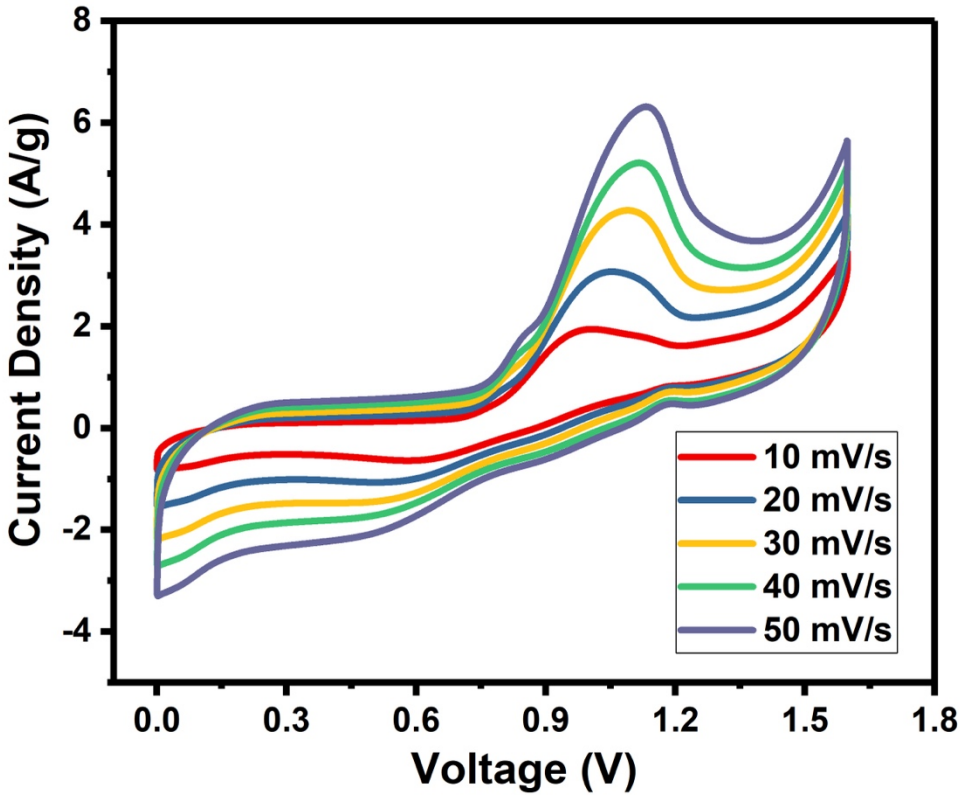

Figure 5.9: CV curves of the AC// $KCo_{0.5}Ni0.4Mn_{0.1}PO_4$ full cell under two-electrode Hybrid Supercapacitor (HSC) operation mode at a potential range of 1.6 V, scanned from 10 mV/s to 50 mV/s.

Figure 5.10 shows the full cell's quantitative charge storage ability through galvanostatic charge-discharge measurements at different current densities within a voltage of 1.6V. Equations (5.11) and (5.12) were used to calculate capacity and capacitance. The Hybrid Supercapacitor's charge storage capacities were found to be 231.7 mAh/g (521 F/g), 198.7

mAh/g (447.07 F/g), 123.5 mAh/g (277.87 F/g), 98.6 mAh/g (221.85 F/g), and 83.57 mAh/g (188.03 F/g) at the respective current densities of 1 A/g, 2 A/g, 5 A/g, 7.5 A/g, and 10 A/g.

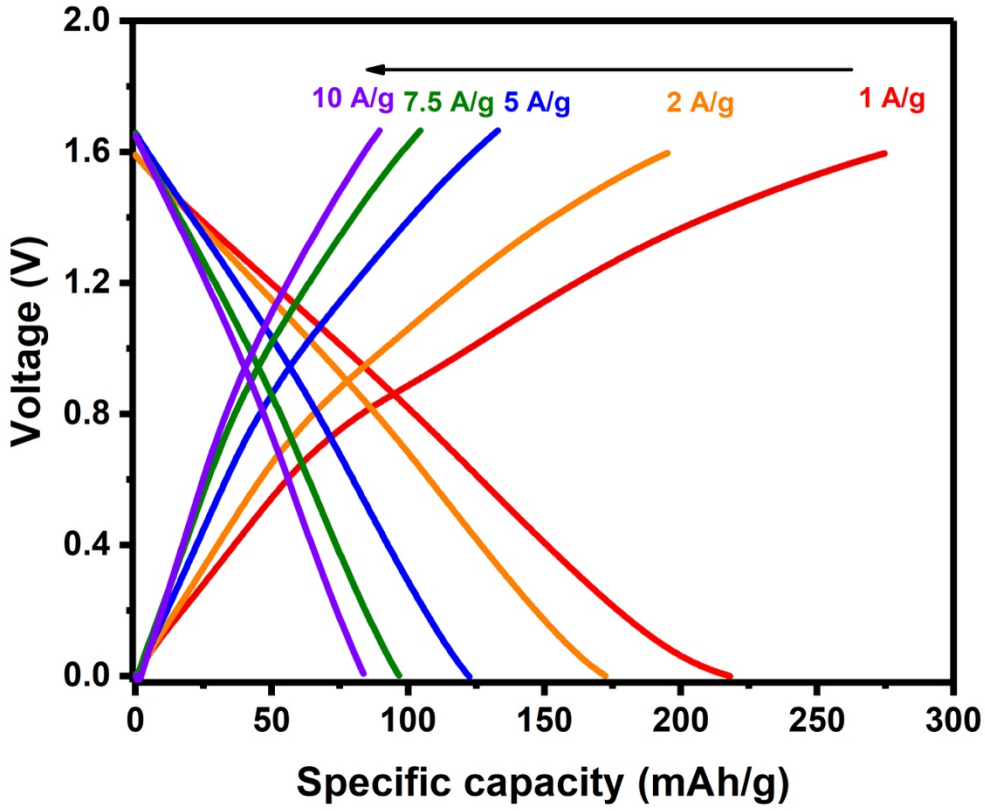

Figure 5.10: Specific capacity of AC// $KCo_{0.5}Ni_{0.4}Mn_{0.1}PO_4$ as HSCs at different current density

The specific energy density (E) and specific power density (P) of the Hybrid Supercapacitor were computed using the following equations.

$$E(Wh/kg) = \frac{1}{2}\frac{C_{HSCs}}{3.6}V^2 \qquad (5.10)$$

$$P(W/kg) = \frac{E*3600}{t_{dis}} \qquad (5.11)$$

Where C_{HSCs} is specific capacitance, V is Potential window and t_{dis} is discharge time.

Figure 5.11 displays a Ragone plot that plots energy density against power capacity at constant current densities. The full cell AC// $KCo_{0.5}Ni0.4Mn_{0.1}PO_4$ showed outstanding performance, reaching a peak energy density of 202.7 Wh/kg at a current rate of 1 A/g (with an accompanying power capacity of about 867.2 W/kg). The full cell exhibited a maximum power density of

9642 W/kg along with an energy density of 65.7 Wh/kg when operated at a current density of 10 A/g.

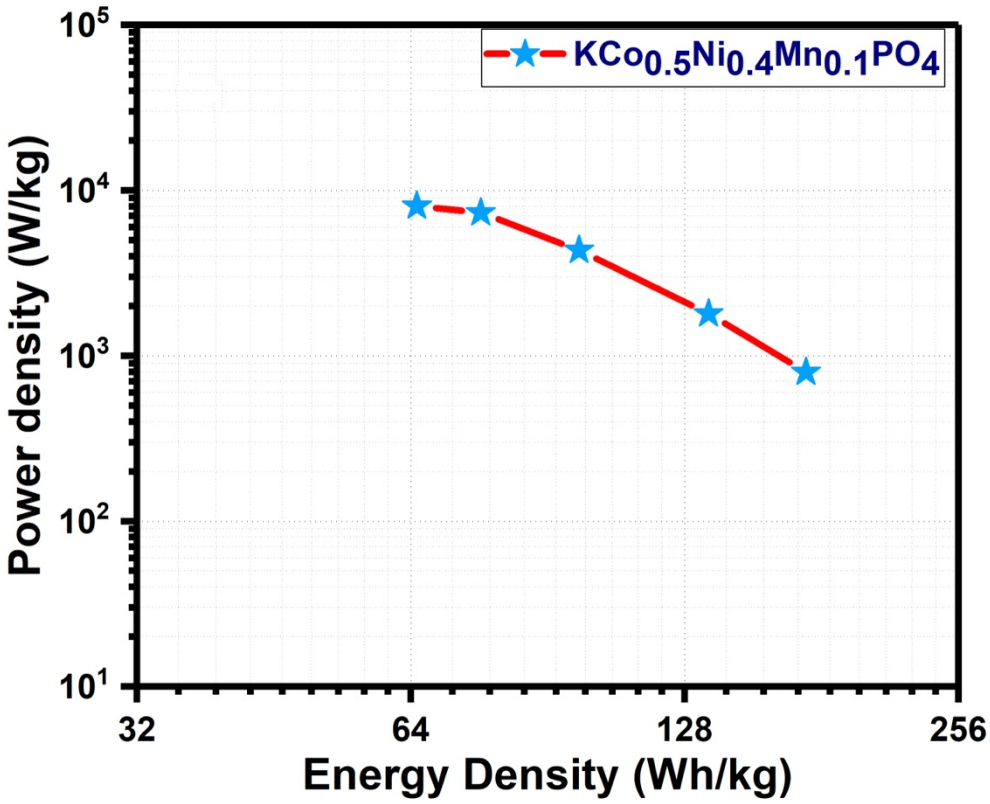

Figure 5.11: Energy density vs power capacity plot at different constant current densities

These great performances in the two-electrode Hybrid Supercapacitor configuration for HSC development clearly point out the efficiency of the $KCo_{0.5}Ni0.4Mn_{0.1}PO_4$ electrode to create advanced Hybrid Supercapacitors.

Table 5.1 Comparative Study of Electrochemical Performances of Cobalt, Nickel and Manganese based Phosphate Electrode Materials in Full Cell

Electrode material (Negative Electrode//Positive Electrode)	Electrolyte	Specific Capacitance	Energy density /Power Density	Ref.
AC//γ-$KCoPO_4$	1M KOH	100 C/g at 0.6 mA/cm^2	ED=28 Wh/kg at PD=1600W/kg	[11]
AC//$KNiPO_4$	2MKOH	168.5 mAh/g (Capacitance: 935 F/g) at 1 A/g	ED=200 Wh/kg PD=819 W/kg	[15]
AC// $NaMn_{1/3}Ni_{1/3}Co_{1/3}PO_4$	2M NaOH	45 F/g at 0.5A/g	ED=15 Wh/kg PD=400 W/kg	[16]
AC// $Co_3(PO_4)_2$	1M NaOH	111.2 F/g at 5mA/cm^2	ED=29.20 Wh/kg at PD= 4687 W/kg	[17]
AC// $Co_3(PO_4)_2 \cdot 8H_2O$	1M KOH	163 F/g at 2mA/cm^2	ED=58.12 Wh/kg at PW=3520 W/kg	[18]
AC//$NH_4NiPO_4 \cdot H_2O$	3M KOH	1513 F/g at 5 A/g	ED= 41.6 Wh/ kg at PD= 375 W/kg	[12]
AC// $NaNiPO_4$	2M NaOH	90 F/g at 0.3A/g	ED= 32 Wh/kg at PD= 300 W/kg	[13]
AC// $KCo_{0.33}Ni_{0.67}PO_4 \cdot H_2O$	1M KOH	227F/g at 1.5A/g	ED=80.64 Wh/kg at PW=8000 W/kg	[14]
AC//$Co_{0.125}Cu_{0.375}Mn_{0.5}(PO_4)_2$	1M KOH	158.5F/g @1A/g	ED=56Wh/kg at PD=6420W/kg	[23]
AC//KCoPO4	2M KOH	387F/g at 1A/g	ED=121.1 Wh/kg at PD= 6945 W/kg	Previous work
AC//$KCo_{0.5}Ni_{0.5}PO_4$	2M KOH	173mAh/g @0.5A/g	ED=183.5Wh/kg at PD=7952W/kg	Previous work
AC//$KCo_{0.5}Ni_{0.4}Mn_{0.1}PO_4$	2M KOH	231 mAh/g at 1A/g	ED=202.7Wh/kg at PD=9642W/kg	This work

5.5 Conclusions

Synthesis done of $KCo_{0.5}Ni0.4Mn_{0.1}PO_4$ powder through the sol-gel auto-combustion method followed by high temperature calcination at 600°C in air, as a two-step process has proven the ability for successful preparation of a strong phosphate-based electrode material. The substitution of Co^{2+} ions in phosphate framework with Ni^{2+} and Mn^{2+} redox-active ions led to their synergistic interaction with Co^{2+}. These interactions played an important role in enhancing the redox-mediated diffusive charge storage, which led to a significantly higher overall charge storage capability. Capacitive-type surface charge storage was also observed on the $KCo_{0.5}Ni0.4Mn_{0.1}PO_4$ electrode, which confirmed their Hybrid storage behavior.

Among the synthesized composition, the $KCo_{0.5}Ni0.4Mn_{0.1}PO_4$ resulted with electrochemical properties, with a specific capacity of 177 mAh/g and a capacitance of 1062 F/g at a current density of 1 A/g. It is due to the ration near 50:40:10 % (Co:Ni:Mn) composition, the charge storage mechanism predominantly observed was intercalative pseudocapacitive behavior rather than storage based on the surface.

For assessing its practical applicability, a full-cell Hybrid Supercapacitor was fabricated using activated carbon as the negative electrode and $KCo_{0.5}Ni0.4Mn_{0.1}PO_4$ as the positive electrode (AC//$KCo_{0.5}Ni0.4Mn_{0.1}PO_4$ cell), resulted with a specific capacity of 231 mAh/g and a capacitance of 521 F/g at a current density of 1 A/g. The AC//$KCo_{0.5}Ni0.4Mn_{0.1}PO_4$ HSC provided an exceptional energy density of 202.7 Wh/kg with a power density of 867.2 W/kg in a 2M KOH aqueous electrolyte within a potential window of 1.6 V at a current rate of 1 A/g. At the same time, with a high current rate, the device was impressive in a power density of 9642 W/kg and managed to store energy up to 65.7 Wh/kg by its current rate at 10 A/g, with excellent cyclic stability.

In summary, $KCo_{0.5}Ni0.4Mn_{0.1}PO_4$ shows superior electrochemical performance, and hence an excellent Hybrid electrode material in Supercapacitors with high promise. Its well-noted

specific capacity along with excellent cycling stability with superior power and energy density makes it highly promising to be used in grid-scale applications for energy storage. The nontoxic, stable material also increases the possibility to be used in modern advanced high-performance energy storage systems, fulfilling the need to store energy and manage energy efficiently.

References

[1] E. Capacitors, “What Are Batteries, Fuel Cells, and Supercapacitors?,” 2004,104,4245-

4270, DOI: 10.1021/cr020730k.

[2] S. Chu and A. Majumdar, “Opportunities and challenges for a sustainable energy future,” *Nature*,2012, 488, 294–303, DOI: 10.1038/nature11475.

[3] R. Eisenberg, “Addressing the Challenge of Carbon-Free Energy,” *ACS Energy Lett.*, 2018, 3, 1521–1522, DOI: 10.1021/acsenergylett.8b00889.

[4] Z. Lv, W. Li, L. Yang, X. J. Loh, and X. Chen, “Custom-Made Electrochemical Energy Storage Devices,” *ACS Energy Lett.*, 2019, 4, 606–614, 2019, DOI: 10.1021/acsenergylett.8b02408.

[5] K. Subramanyan, M. L. Divya, and V. Aravindan, “Dual-carbon Na-ion capacitors: progress and future prospects,” *J. Mater. Chem. A*, vol. 9, no. 15, pp. 9431–9450, 2021, doi: 10.1039/d0ta12099e.

[6] E. Capacitors, “What Are Batteries , Fuel Cells , and Supercapacitors ?,” 2004, doi: 10.1021/cr020730k.

[7] D. Kaufman, K. L. Hudson, and R. Mcclamrock, “and Supercapacitors Begin ?,” vol. 343, no. March, pp. 1210–1212, 2014.

[8] J. Liu, C. Xu, Z. Chen, S. Ni, and Z. X. Shen, “Progress in aqueous rechargeable batteries,” *Green Energy Environ.*, vol. 3, no. 1, pp. 20–41, 2018, doi: 10.1016/j.gee.2017.10.001.

[9] J. Cherusseri, D. Pandey, and J. Thomas, “Symmetric, Asymmetric, and Battery-Type Supercapacitors Using Two-Dimensional Nanomaterials and Composites,” *Batter. Supercaps*, vol. 3, no. 9, pp. 860–875, 2020, doi: 10.1002/batt.201900230.

[10] J. B. Goodenough and P. Singh, “Review-Solid electrolytes in rechargeable electrochemical cells,” *J. Electrochem. Soc.*, vol. 162, no. 14, pp. A2387–A2392, 2015, doi: 10.1149/2.0021514jes.

[11] A. González, E. Goikolea, J. A. Barrena, and R. Mysyk, “Review on supercapacitors:

Technologies and materials," *Renew. Sustain. Energy Rev.*, 2016, 1189–1206, DOI: 10.1016/j.rser.2015.12.249.

[12] Y. Jiang and J. Liu, "Definitions of Pseudocapacitive Materials: A Brief Review," *Energy Environ. Mater.*, 2019, 2, 30–37, 2019, DOI: 10.1002/eem2.12028.

[13] M. Singh, S. Kumar, R. Mondal, P. Singh, R. Prakash, and N. Sharma, "Combustion-Synthesized KNiPO4: A Non-toxic, Robust, Intercalating Battery-Type Pseudocapacitive Electrode for Hybrid Supercapacitors as a Large-Scale Energy Storage Solution," *Energy and Fuels*, 2023, 37,4094–4105, DOI: 10.1021/acs.energyfuels.2c04092.

[14] N. Priyadharsini, A. Shanmugavani, L. Vasylechko, and R. Kalai Selvan, "Sol-gel synthesis, structural refinement, and electrochemical properties of potassium manganese phosphate for supercapacitors," *Ionics (Kiel).*, 2018, 24, 2073–2082, DOI: 10.1007/s11581-018-2449-y.

[15] N. Priyadharsini, S. Surendran, B. Senthilkumar, L. Vasylechko, and R. K. Selvan, "Synthesis and Electrochemical Performances of γ-KCoPO4 Nanocrystals as Promising Electrode for Aqueous Supercapatteries," *ChemElectroChem*, 2019, 6, 369–377, DOI: 10.1002/celc.201801440.

[16] C. Masquelier and L. Croguennec, "Polyanionic (phosphates, silicates, sulfates) frameworks as electrode materials for rechargeable Li (or Na) batteries," *Chem. Rev.*, 2013,113, 6552–6591, DOI: 10.1021/cr3001862.

[17] P. Singh, K. Shiva, H. Celio, and J. B. Goodenough, "Eldfellite, NaFe(SO4)2: an intercalation cathode host for low-cost Na-ion batteries," *Energy Environ. Sci.*, vol. 8, no. 10, pp. 3000–3005, 2015, doi: 10.1039/c5ee02274f.

[18] L. Sharma and A. Manthiram, "Polyanionic insertion hosts for aqueous rechargeable batteries," *J. Mater. Chem. A*, vol. 10, no. 12, pp. 6376–6396, 2022, doi:

10.1039/d1ta11080b.

[19] M. Minakshi, D. Meyrick, and D. Appadoo, “不同锂配比Li_Ni_1_3_Co_1_3_省略_n_1_3_O_2正极材料的合.pdf,” 2013.

[20] Y. Jiang *et al.*, “Transition metal oxides for high performance sodium ion battery anodes,” *Nano Energy*, vol. 5, pp. 60–66, 2014, doi: 10.1016/j.nanoen.2014.02.002.

[21] J. Ding, W. Hu, E. Paek, and D. Mitlin, “Review of Hybrid Ion Capacitors : From Aqueous to Lithium to Sodium,” 2018, doi: 10.1021/acs.chemrev.8b00116.

[22] M. Yang *et al.*, “Effect of nickel doping on the structure, morphology and oxygen evolution reaction performance of Cu-BTC derived CuCoO2,” *Dalt. Trans.*, vol. 51, no. 22, pp. 8757–8765, 2022, doi: 10.1039/d2dt00970f.

[23] G. Wang, Z. Yan, N. Wang, M. Xiang, and Z. Xu, “NiO/Ni Metal-Organic Framework Nanostructures for Asymmetric Supercapacitors,” *ACS Appl. Nano Mater.*, vol. 4, no. 9, pp. 9034–9043, 2021, doi: 10.1021/acsanm.1c01628.

[24] N. B. Velhal *et al.*, “Exploring the Effect of Ultrafast Intensive Pulsed Light (IPL) Annealing on the Structure and Performance of Cobalt Oxide Electrodes for Supercapacitors,” *ACS Appl. Energy Mater.*, vol. 6, no. 14, pp. 7405–7418, 2023, doi: 10.1021/acsaem.3c00656.